

HETEROGENEOUS PHENOMENA OF BUBBLE FLOW IN GAS-FLUIDIZED BEDS

X. F. DONG and A. B. YU

School of Materials Science and Engineering, University of New South Wales, Sydney NSW 2052, Australia

ABSTRACT

Bubbling fluidized beds are used in a variety of power generation and chemical process applications. The formation, breakage and growth of bubbles are related to smooth fluidization, heat exchange and mixture efficiency. The present paper numerically studies heterogeneous phenomena of bubble flow in gas-fluidized beds based on the well established two-fluid model. The modelling system is firstly validated by comparing the theoretical and experimental results. Then, three factors, which possibly affect bubble flow, are considered in the simulation: a) initial bed porosity distribution; b) inlet fluidizing gas velocity distribution; c) solid blocks in a bed. The results show that inlet velocity distribution contributes much to the asymmetry of bubble flow system. The bubble flow pattern and pressure distribution are sensitive to the block arrangement. Mesh block arrangement gives high frequent bubbles and low pressure amplitude. The formation and rising of bubbles under the blocks has been numerically reported. The identification of these flow features is helpful for the control of bubble flow and related heat and mass transfer.

NOMENCLATURE

- A bubble area, m^2
 c compaction modulus (—)
 C_d drag coefficient (—)
 d diameter, m
 D_e equivalent bubble diameter, m
 F interaction force per unit volume, $kg \cdot m^{-2} \cdot s^{-2}$
 g gravitational acceleration, $m \cdot s^{-2}$
 G_0 normalizing unit factor, Pa
 p pressure, Pa
 Re_s Reynolds number, $Re_s = f_s d_s r_g e_g |u_g - u_s| / m_g$
 t time, s
 u interstitial velocity, $m \cdot s^{-1}$

Greek

- ε volume fraction (—)
 ε^* compaction volume fraction (—)
 I identity tensor (—)
 μ viscosity, $kg \cdot m^{-1} \cdot s^{-1}$
 ρ density, $kg \cdot m^{-3}$
 τ stress tensor, Pa
 ϕ shape factor (—)

Subscripts

- g gas
 i identifier (g, s)
 j identifier (g, s)
 s solid

INTRODUCTION

A fluidized bed reactor is a typical example that involves dispersed and dense fluid-particle flow, in which bubbling, turbulent, fast fluidization and dense conveying can occur mainly depending on fluid velocity and particle properties. Because many industrial gas-fluidized beds operate in the bubbling regime, this region has received more attention than any other regimes (Grace, 1982), in which strong heterogeneous flow occurs together with a wide range of solid concentration. The bubbles and solid motion are closely related to mass and heat transfer, particle mixing and efficiency of fluidization beds as chemical reactors. The control and improvement of performance can only come after the bubble behaviour and gas-solid contacting are understood.

In early studies, empirical or semi-empirical correlations are used to indicate the onset of bubbling as summarized by Grace (1982). Later, hydrodynamic approach pioneered by Davidson (1963) provided the foundation for a number of successful two-phase flow models applied to fluidization, from qualitative description to quantitative prediction. In these efforts, gas phase is always thought to be continuous while solid phase may be considered as either continuous or discrete. This is directly reflected in the two popular models in modelling bubbling fluidization i.e. Two-Fluid Model (TFM) (e.g. Jackson, 1963; Anderson and Jackson, 1967; Garg et al., 1975; Gidaspow et al., 1983; Ding et al., 1990; Kuipers et al. 1992a) and Combined Continuum and Discrete Model (CCDM) (e.g. Tsuji et al., 1993; Hoomans et al., 1996; Xu et al., 1997). In CCDM, the motion of individual particles is obtained by solving Newton's equations of motion. The model has the advantage that there is no need for global assumptions on solids such as uniform constituency and constitutive relations. However, for systems with a large number of solid particles, large computer memory size and long computational time are necessary. In TFM, both gas and solid particle are treated as interpenetration continuum media, which is preferable in process modelling and applied research because of its computational convenience. In the model, constitutive equations describing the solid stress are based on the kinetic theory or the data from powder compaction experiments. The former uses the kinetic theory of granular flow, which is often referred to as KTGF. The latter uses the constant solid viscosity and an exponential power law for the particle-particle interaction force, which is referred to as the constant viscosity model (CVM). Recent critical comparison of the performance of CVM and KTGF indicates that both can generate similar results because solid stress is of minor importance compared to the gravity and drag force (van Wachem et al. 2001; Patil et al., 2005). Therefore, only CVM is used in this work.

In the past years, CVM has been widely used to predict the bubble behaviour, such as bubble formation, porosity distribution in the bubbling fluidization bed (e.g. Kuipers et al. 1992b), block influence on bubbles (e.g. Li and Zakkay, 1994), gas and particle properties' influence (e.g. Huttenhuis et al., 1996). However, most of these studies assume the symmetrical flow field so that calculation was done for only half a bed. Asymmetry present in the experiment has been reported by Kuipers et al (1992b), which is argued to be an important cause for the difference between calculated and experimental results. This implies that non-uniform initial and boundary conditions, which possibly induce asymmetries, may significantly affect the bubble behaviour. Witt and Perry (1995) numerically confirmed this consideration with regard to macroscopically asymmetrical initial condition generated by an assumed non-uniform minimum fluidization velocity. Since then, this issue has not been examined seriously.

The purpose of this paper is to present a computational study of the influence of locally asymmetrical initial and boundary conditions on the bubbling fluidization and provide a detailed analysis of bubble behaviour in the bed with different internal block arrangements. The paper is organized as follows: first, details of the CFD formulation are provided, including the numerical model, discretization and solution strategies; second, different test cases are presented which illustrate the effectiveness of modelling system; finally, the effects of non-uniform initial/boundary conditions and internal blocks on the bubble flow are investigated.

MATHEMATICAL MODELLING

Governing equations

A model for gas–solid two-phase incompressible flow can be formulated based on different averaging approaches, i.e. space, time or statistical averaging (Soo, 1991). These approaches derive a similar set of balance equations that are closed by specifying constitutive relations, such as a gas-solid momentum transfer and distinct phase stress tensor. In this work, the employed equations are generalized from Navier-Stokes equations (Kuipers et al., 1992a), in which two phases are described in terms of separate conservation equations with a shared pressure and appropriate interaction terms representing the coupling between the phases. The model is the same as Model A of Gidaspow (1994), which is preferable for gas-solid two phase flow (Hudson and Harris, 2006). Thus, the continuity and momentum equations for the two-dimensional, isothermal, viscous two-phase flow in a fluidized bed can be, respectively, written in the following general form:

Conservation of mass of phase i

$$\frac{\partial(\mathbf{r}_i \mathbf{e}_i)}{\partial t} + \nabla \cdot (\mathbf{r}_i \mathbf{e}_i \mathbf{u}_i) = 0 \quad (1)$$

Conservation of momentum of phase i

$$\frac{\partial(\mathbf{r}_i \mathbf{e}_i \mathbf{u}_i)}{\partial t} + \nabla \cdot (\mathbf{r}_i \mathbf{e}_i \mathbf{u}_i \mathbf{u}_i) = -\mathbf{e}_i \nabla p + \nabla \cdot \mathbf{t}_i + \mathbf{r}_i \mathbf{e}_i \mathbf{g} + \mathbf{F}_i^j \quad (2)$$

where

$$\mathbf{e}_s + \mathbf{e}_g = 1 \quad (3)$$

The constitutive equations necessary for closure of the above equations are listed in Table 1.

$$\begin{aligned} \mathbf{t}_g &= -\frac{2}{3} \mathbf{e}_g \mathbf{m}_g (\nabla \cdot \mathbf{u}_g) \mathbf{I} + \mathbf{e}_g \mathbf{m}_g [(\nabla \mathbf{u}_g) + (\nabla \mathbf{u}_g)^T] \\ \mathbf{t}_s &= -\left[p_s + \frac{2}{3} \mathbf{e}_s \mathbf{m}_s (\nabla \cdot \mathbf{u}_s) \right] \mathbf{I} + \mathbf{e}_s \mathbf{m}_s [(\nabla \mathbf{u}_s) + (\nabla \mathbf{u}_s)^T] \\ p_s &= \frac{G_0}{c} \exp[c(\mathbf{e}_s - \mathbf{e}_s^*)] \\ \mathbf{F}_g^s &= -\mathbf{F}_s^g = -\left[150 \frac{\mathbf{e}_s^2}{\mathbf{e}_g} \frac{\mathbf{m}_g}{(\mathbf{f}_s d_s)^2} + 1.75 \mathbf{e}_s \frac{\mathbf{r}_g}{\mathbf{f}_s d_s} |\mathbf{u}_g - \mathbf{u}_s| \right] (\mathbf{u}_g - \mathbf{u}_s) \quad \mathbf{e}_g \leq 0.8 \\ &= -\frac{3}{4} C_d \frac{\mathbf{e}_g \mathbf{r}_g \mathbf{e}_s}{\mathbf{f}_s d_s} |\mathbf{u}_g - \mathbf{u}_s| \mathbf{e}_s^{-2.65} (\mathbf{u}_g - \mathbf{u}_s) \quad \mathbf{e}_g > 0.8 \\ \text{where } C_d &= \begin{cases} \frac{24}{\text{Re}_s} & \dots \text{Re}_s \leq 1 \\ \frac{24}{\text{Re}_s} [1 + 0.15 \text{Re}_s^{0.687}] & \dots 1 < \text{Re}_s \leq 1000 \\ 0.44 & \dots 1000 < \text{Re}_s \end{cases} \end{aligned}$$

Table 1: Constitutive equations

where G_0 , c and \mathbf{e}_s^* have been taken as 1, 100 and 0.56.

Gas turbulence based on a standard k - ϵ model (Wilcox, 1993) is also considered in the simulation.

Numerical technique

The finite difference method is used to solve the two sets of conservation equations. The solution domain is subdivided into computational cells (control volumes) using a staggered grid in which the pressure and all other scalar variables are stored at the cell centres, and the velocity components are stored at the control volume faces (Patankar, 1980). Fully implicit scheme is used for the partial derivative in time. Convective terms are discretized by the deferred correction method (Khosla and Rubin, 1974), which combines higher (2nd) and lower (1st) order schemes. For the discretization of viscous transport terms in the momentum equations, the central finite difference approximation with second-order spatial truncation error has been used. The Tridiagonal Matrix Algorithm (TDMA) is used for solving the discretised equations in the sparse linear system.

Due to strong coupling between gas and solid phases caused by the interphase drag, the implicit IPSA algorithm (Spalding, 1980) is used and enhanced with Partial Elimination Algorithm (PEA) to decouple the drag and accelerate convergence. Modification of the solution of volume fraction has been done to guarantee the boundedness of the volume fraction (Oliveira and Issa, 2003) and enhance the robustness (Karema and Lo, 1999) when gas-solid flow is computed over a wide range of concentration.

Boundary and computational conditions

At the impenetrable wall, a no slip boundary condition is applied to gas phase and a partial slip boundary condition for solid phase in this work. At the inlet, gas flowrate is specified. At the outlet, a Neumann boundary condition is applied, i.e variable gradient is zero and global mass continuity is guaranteed. Moreover, a static pressure is specified at the outlet boundary condition.

Variable	values
Minimum fluidization porosity	0.402
Minimum fluidization velocity	0.25 m·s ⁻¹
Orifice velocity	10 m·s ⁻¹
Particle diameter	5×10 ⁻⁴ m
Gas density	1.2 kg·m ⁻³
Gas viscosity	1.85×10 ⁻⁵ Pa·s
Particle density	2660 kg·m ⁻³
Solid viscosity	1 Pa·s
Orifice diameter	1.5×10 ⁻² m
Bed width	0.585 m
Initial bed height	0.50 m
X-grid size	5×10 ⁻³ , 1.25×10 ⁻² m
Y-grid size	1.25×10 ⁻² m
Time step	1.0×10 ⁻⁴ s

Table 2: Computational conditions

Computations are performed mainly under the conditions used by Kuipers et al. (1991). These conditions are given in Table 2. Two grid structures, consisting of 47×80 and 117×80 cells, are used separately for the cases without blocks and with blocks. The detailed dimensions of bed geometry and initial particle condition are shown in Fig. 1. The top of the bed is exposed to the atmosphere. Initially the fluidizing gas, introduced at the bottom of the bed at the minimum fluidization velocity, flows in the vertical direction and leaves the bed at the top. Subsequently, secondary gas is injected through the orifice at the centre of the bed.

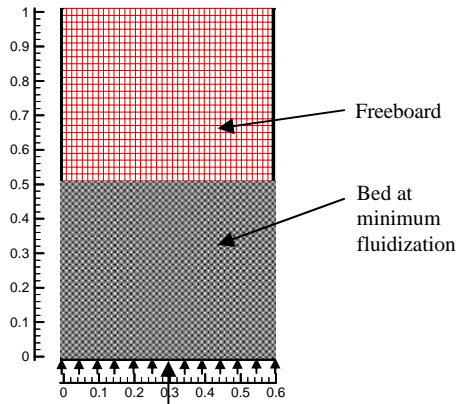


Figure 1: Computational domain.

3. RESULTS AND DISCUSSION

3.1 Validation of modelling system

The numerical predictions of bubble injection into fluidized beds are qualitatively and quantitatively compared to the experimental data of Kuipers et al. (1991, 1992b) and Rowe et al. (1964).

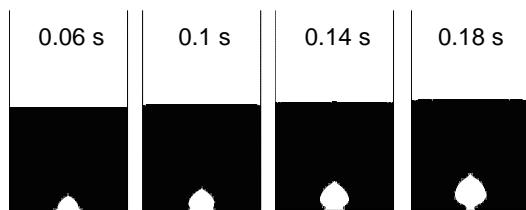


Figure 2: Calculated bubble growth at a single orifice.

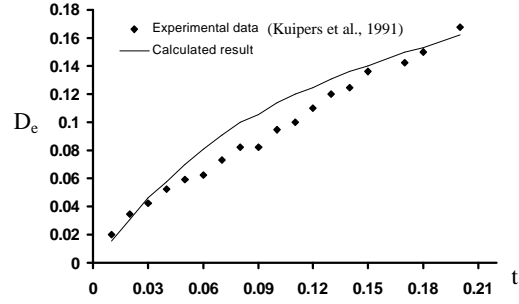


Figure 3: Calculated and experimental bubble size as a function of time.

Fig. 2 shows the formation process of a large bubble. The bubble has been defined to correspond to a porosity contour of value 0.85, according to the computational and experimental observations of Kuipers et al. (1991). Therefore, only two regions are demonstrated in the figure: white ($\epsilon_g \geq 0.85$) and black ($\epsilon_g < 0.85$). From zero to 0.18 second, the void forms, propagates and finally generates a bubble with an equivalent bubble diameter of 0.15 m. A detailed comparison between calculated and measured bubble diameter is shown in Fig. 3, in which D_e is calculated from $D_e = \sqrt{4A/p}$. The calculated bubble sizes are reasonably comparable to the measured values.

The isoporosity contours shown in Fig. 4(b) have also been obtained by simple linear interpolation of the time-averaged calculated solid volume fraction within 1st second. Figure 4(a) shows the time-averaged measured void fractions in the bed for the same jet velocity (Kuipers et al., 1991b), in which a symmetry assumption for the measurement has been made. A comparison of these profiles shows that the experimental and the calculated profiles are very similar. Two regions can be identified, i.e. spouted and emulsion region. However, there are small discrepancies which are considered to be mainly from the inaccuracy of some empirical treatments employed in the model and asymmetrical phenomena existing in the experiments. For example, asymmetrical solid motion can sweep away the possible solid buildup at the centre so that the experimental isoporosity contours are flat near the centreline of the bed.

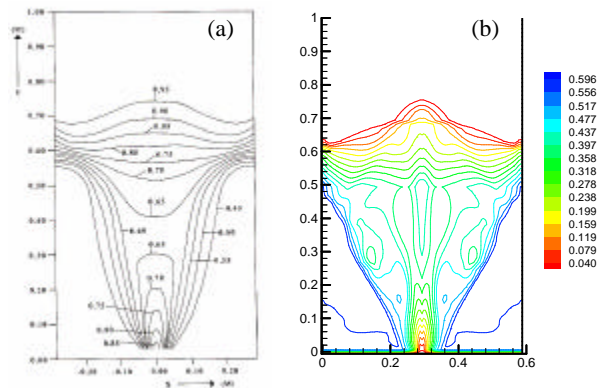


Figure 4: Comparison of experimental and calculated time-averaged porosity: (a) experimental; (b) calculated.

A qualitative comparison of the calculated and measured results has also been done for the rising process of a single bubble. Fig. 5 shows the calculated rising process of a single bubble. A bubble was introduced into a bed maintained at minimum fluidization conditions via a jet

with a gas velocity ($10 \text{ m}\cdot\text{s}^{-1}$) much higher than the minimum fluidization velocity. After the formation of the bubble (0.2 s), the jet velocity was reduced to the minimum fluidization velocity. The bubble subsequently detaches and moves up to the bed surface. The growth and propagation of the bubble occur during rising. An evident wake exists at the bottom of the bubble. Finally the bubble bursts out at the surface of fluidized bed. The whole process can be compared qualitatively to the measured single bubble rise process (Fig. 6) (Rowe et al., 1964). Especially, at the final stage, when the bubble bursts out, gas void spreads at the top, solid particles in the wake rush up inertially and then settle down. The calculated results reproduce this process realistically.

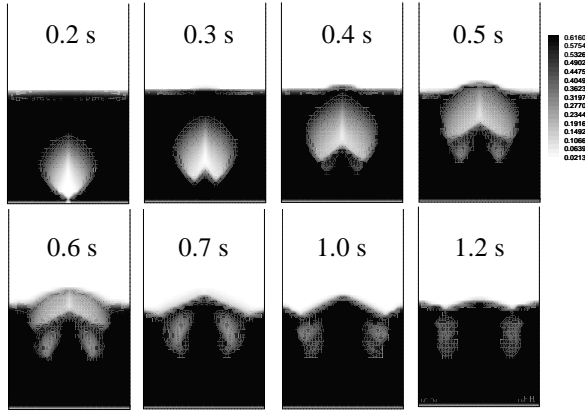


Figure 5: Snapshots of the gas volume fraction when a single bubble rises.

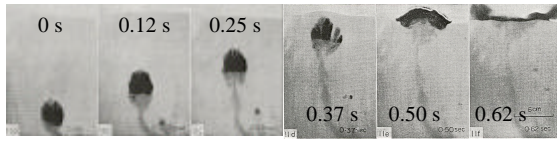


Figure 6: A single bubble rise (Rowe et al., 1964).

3.2 Effect of non-uniform initial porosity

In the previous cases, idealistic symmetrical initial/boundary conditions are given. However, in practice, absolute symmetrical condition is not possible. These conditions may induce asymmetrical flow phenomena in the experiment (Kuipers et al., 1992b). In this study, various attempts have been made to quantitatively analyse possible factors inducing asymmetrical bubble flow. Firstly, initial porosity condition is determined to be randomly distributed and the other conditions are the same as that used in Fig 2. Fig. 7 shows the statistical distribution of initial solid volume fraction, which complies with Gaussian distribution (German, 1989). Macroscopically speaking, initial average solid volume fraction is symmetrically distributed, but locally asymmetrical, as shown in Fig. 8(b).

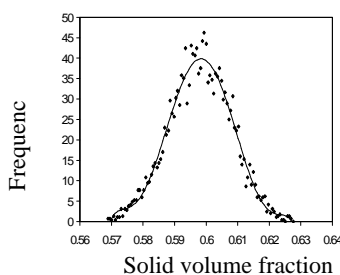


Figure 7: Solid volume fraction distribution.

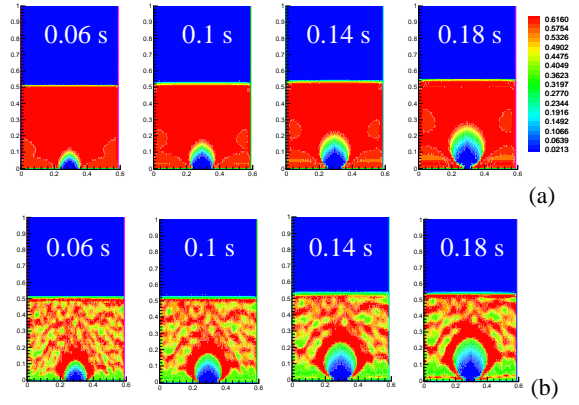


Figure 8: Comparison of bubble sizes for uniform (a) and non-uniform (b) initial porosity distribution.

Within 0.18 s, a detailed comparison of calculated bubble sizes in non-uniform and uniform porosity conditions is given in Fig. 8. During this period, one large bubble is generated around the orifice. As shown in Fig. 8(b), when high speed gas is injected into the bed with a random porosity distribution, a bubble is formed smoothly and symmetrically. A dense particle region forms at the bubble surface. Bubble size and shape can be compared to that with uniform initial distribution (Fig. 8(a)). It indicates that the bubble formation is mainly controlled by upstream gas flow. Before the free bubbling occurs, time-averaged porosity distribution within the first second is also shown in Fig. 9(a), which is almost the same as that shown in Fig. 4(b). All of these show that the initial random porosity distribution has little effect on the bubble flow in terms of bubble size and porosity distribution during the period of the formation and propagation of a start-up bubble.

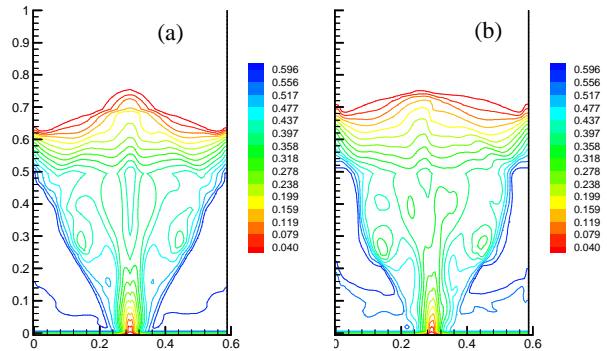


Figure 9: Comparison of predicted time-averaged porosity maps for two cases (within 1st second) with non-uniform (a) initial porosity, and (b) fluidizing gas velocity.

3.3 Effect of non-uniform fluidizing gas velocity

Similar to the above treatment, a non-uniform fluidizing gas velocity distribution is given while other conditions are fixed as provided in Table 2. Fig. 10 shows the corresponding magnitude and frequency distribution of inlet fluidizing gas velocity. Compared to the influence of non-uniform porosity, non-uniform velocity distribution is inclined to destroy the bubble symmetrical flow easily. As shown in Fig. 9(b), time-averaged porosity distribution within 1st second is evidently asymmetrical. It means that, during this period, solid particle can flow across the centreline. A flat iso-porosity contour at the surface can be observed, instead of upward curve shown in Fig. 9(a). It partially proves the assumption made by Kuipers et al. (1992b) about flat iso-porosity distribution in the

experiment is due to the cross flow of solid particle at the centre of the bed, which is also a main reason for the discrepancy between calculated and measured data. Because it is difficult to achieve the absolute symmetrical condition in the experiment, this discrepancy can not be avoided in nature.

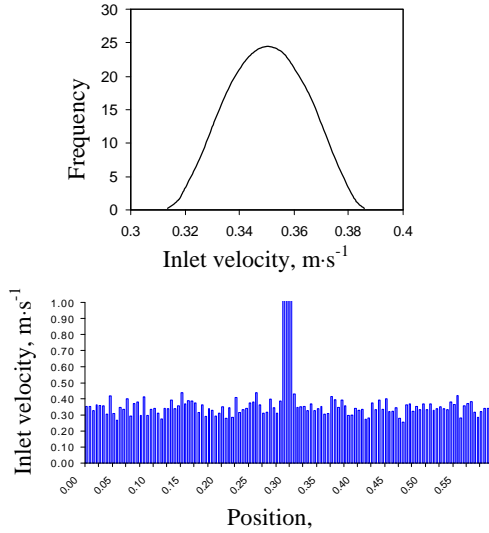


Figure 10: Inlet fluidizing gas velocity distribution.

The numerical snapshots (Fig. 11) further demonstrate this asymmetrical process. Once asymmetrical phenomena are produced, it can not be suppressed and tends to be amplified with time, leading to the formation of complicated flow pattern in a fluidized bed. However, the effect of non-uniform condition on the first bubble formation is not evident. It implies that data obtained during the bubble formation can better validate the credibility of constitutive relation used in the model without the disturbance of possible non-uniform initial/boundary conditions in the experiment.

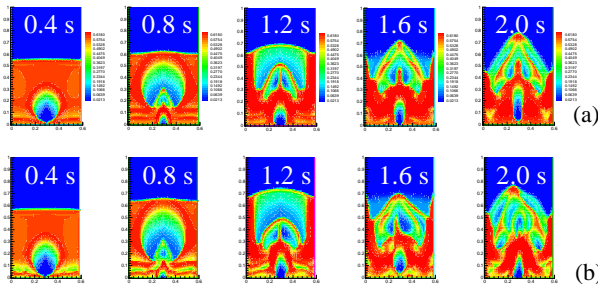


Figure 11: Comparison of bubble flow patterns for uniform (a) and non-uniform (b) inlet gas velocity distribution.

3.4 Effect of internal solid blocks in a bed

Except for the initial/boundary conditions, internal blocks can be another main influence factor to breakup bubbles and promote “smoother” fluidization. They can be heat-exchange pipes in a fluidization bed. In order to investigate their effects on the bubble flow, three block arrangements are considered as shown in Fig. 12, i.e. mesh, inline and staggered arrangements, using uniform initial/boundary conditions given in Table 2. Fig. 13 compares the flow patterns at 2nd second in terms of porosity distribution. The results show that once blocks are introduced into the bed, central jet flow is evidently

confined. When gas and solid particles pass through the blocks, the bubbles break up and re-coalesce, together with increased flow resistance. The different arrangements produce quite different flow patterns. For the inline arrangement, gas can flow easily through the gap between blocks near the centre so that a relative high void almost penetrates through the bed centre. For the mesh case, the mesh plays a role as a filter and the large bubble is difficult to go through. Staggered block arrangement makes the bubble split into numerous small bubbles scattered in the bed. As a typical example, the bed with staggered blocks shows that high voids (bubbles) are easily formed below the blocks, which are similar to the observations (Glass and Harrison, 1964). These bubbles are not stable. Once they get to a certain size, they will leave the region under the blocks and rise up. Some of them will disappear during the rising process, and some can continuously go up to the bed surface and finally burst out. The upper surface of the blocks was intermittently covered by the defluidized particles which can be swept away during each bubble transit. However, for inline arrangement, the defluidized particles on the central blocks are hardly removed due to the idealistic symmetrical fluid flow and high flow resistance at the centreline.

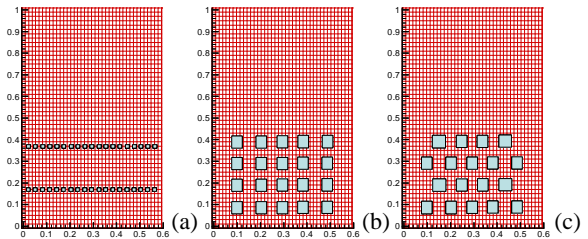


Figure 12: Arrangement of internal blocks: (a) mesh; (b) inline; (c) staggered.

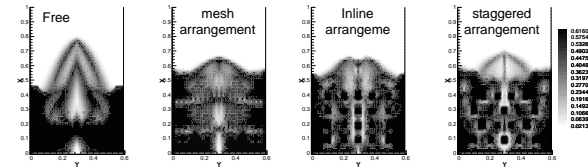


Figure 13: Comparison of porosity distribution as $t = 2$ s.

Porosity variations with time just above the orifice are shown in Fig. 14. Generally, the time for the first bubble formation is the longest. Subsequently, bubble can be regularly generated. Mesh arrangement makes bubble frequency increase. Inline case influences the bubble formation the least. Compared to the above two cases, staggered arrangement is likely to blur the bubble, which also can be demonstrated in the power spectrum analysis as shown in Fig. 15. Correspondingly, pressure variations (Fig. 16) show that pressure drop with the blocks is higher than that without blocks due to the increased friction between gas-solid and blocks. Among them, mesh block induces the highest frequency of pressure variation and the lowest amplitude.

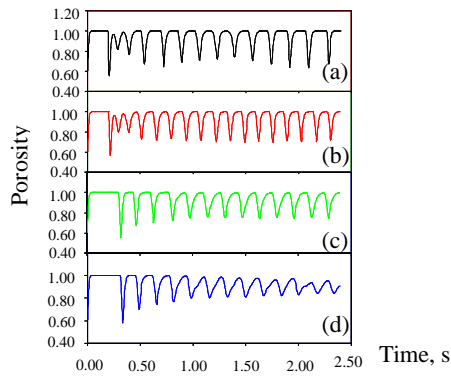


Figure 14: Variation of porosity with time at the different block arrangements: (a) free; (b) mesh; (c) inline; (d) staggered.

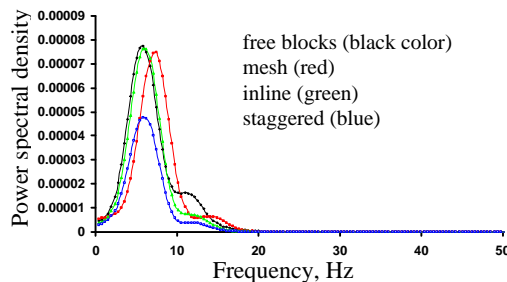


Figure 15: Power spectrum density analysis of porosity fluctuation for the different block arrangements.

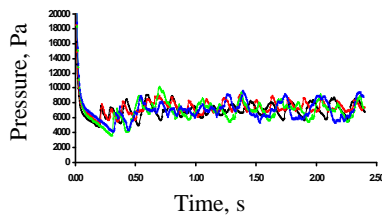


Figure 16: Variation of inlet pressure with time for the different block arrangements: (a) free (black color); (b) mesh (red); (c) inline (green); (d) staggered (blue).

CONCLUSIONS

Two fluid flow model has been employed to study the heterogeneous phenomena of bubble flow in a two-dimensional fluidized bed, with its validity confirmed by comparing numerical simulations and experimental results under different conditions. The effects of non-uniform initial/boundary conditions in terms of local asymmetry and internal blocks on the bubble flow have been studied. The results show that non-uniform initial/boundary conditions have little effect on the first bubble formation. However, when the bubble rises up, a non-uniform inlet velocity distribution tends to make an asymmetrical bubble flow easily, which is responsible for a flat time-averaged porosity contour at the bed surface. Internal blocks can increase bed pressure drop, break up large bubbles and help generate small bubbles. Especially, mesh blocks produce a high frequency of bubbles and low pressure amplitude around the orifice.

ACKNOWLEDGEMENTS

The authors are grateful to Australian Research Council for the financial support of this work. The authors would like to thank Dr. S.J Zhang for valuable discussion.

REFERENCES

- ANDERSON, T.B. AND JACKSON, R.A., (1967), "A fluid mechanical description of fluidized beds", *Industrial & Engineering Chemistry Fundamentals*, **6**, 527-539.
- DAVIDSON, J.F., *Fluidised Particles*, Cambridge University Press, Cambridge U.K., 1963.
- DING, J. AND GIDASPOW, D., (1990), "A bubbling fluidization model using kinetic-theory of granular flow", *AIChE Journal*, **36**, 523-538.
- GARG, S.K. AND PRITCHETT, J.W., (1975), "Dynamics of gas-fluidized beds", *Journal of Applied Physics*, **46**, 4493-4500.
- GERMAN, R.M., (1989), *Particle Packing Characteristics*, Metal Powder Industries Federation, Princeton, N.J.
- GIDASPOW, D., *Multiphase Flow and Fluidization*, Academic Press, 1994.
- GIDASPOW, D. AND ETTEHADIEH, B., (1983), "Fluidization in two-dimensional beds with a jet .2. hydrodynamic modeling", *Industrial & Engineering Chemistry Fundamentals*, **22**, 193-201.
- GRACE, J.R., *Fluidised-bed hydrodynamics*, *Handbook of Multiphase Systems*, Heteroni, G. (eds), McGraw Hill, New York, 1982
- HOOMANS, B.P.B., KUIPERS, J.A.M., BRIELS, W.J. AND VAN SWAAIJ, W.P.M., (1996), "Discrete particle simulation of bubble and slug formation in a two-dimensional gas-fluidized bed: a hard-sphere approach", *Chemical Engineering Science*, **51**, 99-118.
- HUDSON, J. AND HARRIS, D., (2006), "A high resolution scheme for Eulerian gas-solid two-phase isentropic flow", *Journal of Computational Physics*, **216**, 494-525.
- HUTTENHUIS, P.J.G., KUIPERS, J.A.M. AND VANSWAAIJ, W.P.M., (1996), "The effect of gas-phase density on bubble formation at a single orifice in a two-dimensional gas-fluidized bed", *Chemical Engineering Science*, **51**, 5273-5288.
- JACKSON, R., (1963), "The mechanics of fluidized beds: part I: the stability of the state of uniform fluidisation", *Transactions Institute Chemistry Engineers*, **41**, 13-21.
- KAREMA, H. AND LO, S., (1999), "Efficiency of interphase coupling algorithms in fluidized bed conditions", *Computers & Fluids*, **28**, 323-360.
- KHOSLA, P.K. AND RUBIN, S.G., (1974), "A diagonally dominant second-order accurate implicit scheme", *Computers and Fluids*, **2**, 207-209.
- KUIPERS, J.A.M., PRINS, W. AND VAN SWAAIJ, W.P.M., (1991), "Theoretical and experimental bubble formation at a single orifice in a two-dimensional gas-fluidized bed", *Chemical Engineering Science*, **46**, 2881-2894.
- KUIPERS, J.A.M., VAN DUIN, K.J., VAN BECKUM, F.P.H. AND VAN SWAAIJ, W.P.M., (1992a), "A numerical model of gas-fluidized beds", *Chemical Engineering Science*, **47**, 1913-24.
- KUIPERS, J.A.M., TAMMES, H., PRINS, W. AND VAN SWAAIJ, W.P.M., (1992b), "Experimental and theoretical porosity profiles in a two-dimensional gas-fluidized bed with a central jet", *Powder Technology*, **71**, 87-99.
- LI, C. AND ZAKKAY, V., (1994), "Hydrodynamics and erosion modeling of fluidized bed combustors", *Journal of Fluids Engineering*, **116**, 746-755.

OLIVEIRA, P.J. AND ISSA, R.I., (2003), "Numerical aspects of an algorithm for the Eulerian simulation of two-phase flows", *International Journal for Numerical Methods in Fluids*, **43**, 1177-1198.

PATANKAR, S.V., *Numerical heat transfer and fluid flow*, McGraw-Hill, New York, 1980.

PATIL, D.J., ANNALAND, M.V. AND KUIPERS, J.A.M., (2005), "Critical comparison of hydrodynamic models for gas-solid fluidized beds - Part I: bubbling gas-solid fluidized beds operated with a jet", *Chemical Engineering Science*, **60**, 57-72.

ROWE, P.N., PARTRIDGE, B.A. AND LYALL, E., (1964), "Cloud formation around bubbles in gas fluidized beds", *Chemical Engineering Science*, **19**, 973-985.

SOO, S.L., (1991), "Comparisons of formulations of multiphase flow", *Powder Technology*, **66**, 1-7.

SPALDING, D.B., "Numerical computation of multiphase fluid flow and heat transfer, *Recent Advances in Numerical Methods in Fluids*", Taylor, C., Morgan, K. (eds), Pineridge Press, Swansea, 1980.

TSUJI, Y., KAWAGUCHI, T. AND TANAKA, T., (1993), "Discrete particle simulation of two-dimensional fluidized bed", *Powder Technology*, **77**, 79-87.

VAN WACHEM, B.G.M., SCHOUTEN, J.C., van den Bleek, C.M., Krishna, R. and Sinclair, J.L., (2001), "Comparative analysis of CFD models of dense gas-solid systems", *AIChE Journal*, **47**, 1035-1051.

WILCOX, D.C., *Turbulence Modelling for CFD*, DCW Industries, La Canada, 1993.

WITT, P.J. and PERRY, J.H. (1995), "A study in multiphase modelling of fluidised beds", *Proceedings of computational techniques and applications: CTAC95*, Melbourne, Australia, July 11-13.

XU, B.H. AND YU, A.B., (1997), "Numerical simulation of the gas-solid flow in a fluidized bed by combining discrete particle method with computational fluid dynamics", *Chemical Engineering Science*, **52**, 2785-2809.